Theor. Comput. Fluid Dyn. (2007) 21: 369–380
DOI 10.1007/s00162-007-0054-1

ORIGINAL ARTICLE

Yongqi Wang · Tasawar Hayat · Kolumban Hutter

Peristaltic flow of a Johnson-Segalman fluid through a deformable tube

Received: 3 March 2003 / Accepted: 6 June 2007 / Published online: 21 July 2007

Abstract To understand theoretically the flow properties of physiological fluids we have considered as a model the peristaltic motion of a Johnson–Segalman fluid in a tube with a sinusoidal wave traveling down its wall. The perturbation solution for the stream function is obtained for large wavelength and small Weissenberg number. The expressions for the axial velocity, pressure gradient, and pressure rise per wavelength are also constructed. The general solution of the governing nonlinear partial differential equation is given using a transformation method. The numerical solution is also obtained and is compared with the perturbation solution. Numerical results are demonstrated for various values of the physical parameters of interest.

Keywords Peristaltic flow · Perturbation solution · Transformation method · Numerical method · Johnson–Segalman fluid

PACS 47.50.-d

1 Introduction

Peristaltic pumping is a form of fluid transport that occurs when a progressive wave of area contraction or expansion propagates along the length of an extensible tube containing a liquid. In physiology, it appears to be a major mechanism for urine transport in the ureter, in swallowing food through the esophagus, transport of lymph in the lymphatic vessels, and in the vasomotion of small blood vessels such as arterioles, venules, and capillaries. Technical roller and finger pumps also operate according to this mechanism.

Since the first investigation by Latham [1], several theoretical and experimental attempts have been made to understand this peristaltic action in different situations. A review of the early literature is presented in Jaffrin and Shapiro [2]. The theoretical investigations of peristaltic motion by Burns and Parkes [3], Barton

Communicated by M.Y. Hussaini

Y. Wang (✉)
Chair of Fluid Dynamics, Department of Mechanical Engineering, Darmstadt University of Technology, Hochschulstrasse 1, 64289 Darmstadt, Germany
E-mail: wang@fdy.tu-darmstadt.de

Y. Wang
Institute of Geotechnical Engineering, Universität für Bodenkultur, Feistmantelstr. 4, 1180 Vienna, Austria

T. Hayat
Mathematics Department, Quaid-i-Azam University, Islamabad 45320, Pakistan

K. Hutter
VAW, ETH Zürich, Gloriastrasse 37, 8092 Zürich, Switzerland

and Raymor [4], Chow [5], Shapiro et al. [6], Jaffrin [7], Liron [8], and Takabatake and Ayukawa [9] have excited some interest in recent years. However, these studies are confined to Newtonian fluids. Some of the theoretical and experimental studies considering blood as a non-Newtonian fluid are discussed in references [10–14]. The peristaltic transport of non-Newtonian fluids is also discussed by Siddiqui et al. [15] and Siddiqui and Schwarz [16,17], Böhme and Friedrich [18], Misra and Pandey [19,20], and Hayat et al. [21,22].

In this paper, the peristaltic flow of a Johnson–Segalman fluid in a tube is considered, which can be used to explain the *spurt* phenomenon [23–25]. Experimentalists usually associate spurt with slip at the wall [26–31]. The present analysis is based on an adaptation of the channel geometry to cylindrical geometry since small glandular ducts and other tracts of the body involving peristalsis are approximately cylindrical in shape. Thus, the axisymmetric case seems more realistic physiologically than the channel case. With this fact in view, the perturbation solution, general analytical solution, and numerical solution are investigated for the flow in a tube. The presented analysis holds for the large-wavelength case, for which normal-stress effects and memory effects of a viscoelastic Johnson–Segalman fluid are excluded and the fluid behaves like a nonlinear viscometric flow. For the perturbation solution, the expressions for the stream function, axial velocity, pressure gradient and pressure rise over a wavelength are derived, valid for small Weissenberg number. The transformation method is used to find the general analytical solution of the governing nonlinear partial differential equation arising from the momentum equation. Finally, the numerical solution is obtained and compared with the perturbation solution. Several results of interest are obtained as particular cases of the presented analysis.

2 Basic equations

We choose the Johnson–Segalman fluid, which is characterized by the constitutive equations [32]

$$\begin{aligned} &\bar{\boldsymbol{\sigma}} = -p\mathbf{I} + \bar{\boldsymbol{\tau}}, \qquad \bar{\boldsymbol{\tau}} = 2\mu\bar{\mathbf{D}} + \bar{\mathbf{S}}, \\ &\bar{\mathbf{S}} + m\left[\frac{\mathrm{d}\bar{\mathbf{S}}}{\mathrm{d}t} + \bar{\mathbf{S}}\left(\bar{\mathbf{W}} - a\bar{\mathbf{D}}\right) + \left(\bar{\mathbf{W}} - a\bar{\mathbf{D}}\right)^{T}\bar{\mathbf{S}}\right] = 2\eta\bar{\mathbf{D}}, \end{aligned} \tag{1}$$

in which $\bar{\boldsymbol{\sigma}}$ is the Cauchy stress tensor, p is the pressure, $\mathbf{I}$ the unit tensor, $\bar{\boldsymbol{\tau}}$ the extra stress tensor, $\bar{\mathbf{S}}$ the extra stress, which takes into account the truly nonlinear viscoelastic behavior of the fluid, μ the Newtonian viscosity, η the elastic shear modulus, m the relaxation time, and a is called the slip parameter. $\bar{\mathbf{D}}$ and $\bar{\mathbf{W}}$ are the symmetric and skew-symmetric parts of the velocity gradient ($\bar{\mathbf{L}} = \operatorname{grad}\bar{\mathbf{V}}$), respectively, and are given by

$$\bar{\mathbf{D}} = \tfrac{1}{2}\left(\bar{\mathbf{L}} + \bar{\mathbf{L}}^{T}\right), \quad \bar{\mathbf{W}} = \tfrac{1}{2}\left(\bar{\mathbf{L}} - \bar{\mathbf{L}}^{T}\right). \tag{2}$$

We note that, for $a = 1$ and $\mu = 0$, the model (1) reduces to the Maxwell model, and that when $m = 0$ it becomes Newtonian.

The equations of continuity and momentum in the absence of body forces are

$$\operatorname{div}\bar{\mathbf{V}} = 0, \qquad \rho\frac{\mathrm{d}\bar{\mathbf{V}}}{\mathrm{d}\bar{t}} = \operatorname{div}\bar{\boldsymbol{\sigma}}, \tag{3}$$

where ρ is the density and $\bar{t}$ is the time.

3 Mathematical formulation

We consider the flow in a circular cylindrical tube with a sinusoidal wave of small amplitude traveling down the wall. The dimensional wall equation is given by

$$\bar{R}_{\mathrm{wall}} = \bar{h}\left(\bar{Z}, \bar{t}\right) = h_0 + b\sin\left[\frac{2\pi}{\lambda}\left(\bar{Z} - c\bar{t}\right)\right], \tag{4}$$

and is shown graphically in Fig. 1. Here h_0 is the average radius of the original undisturbed tube, b is the amplitude of the wave, λ is the wavelength, and c is the wave speed. $\bar{R}$ and $\bar{Z}$ are the cylindrical coordinates with $\bar{Z}$ measured along the axis of the tube and $\bar{R}$ in the radial direction. Let $\bar{U}$ and $\bar{W}$ be the velocity components in the radial and axial directions, respectively. We further assume that the wall is extensible.

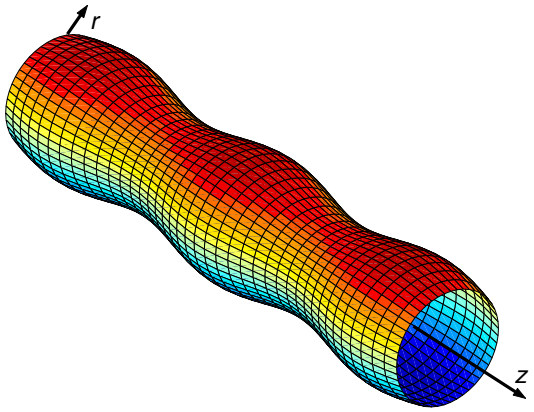

Fig. 1 Schematic diagram of the cylindrical tube

In the laboratory frame $\left(\bar{R}, \bar{Z}\right)$, the flow in the tube is unsteady. In order to carry out a steady-state analysis, we move to the wave frame $(\bar{r}, \bar{z})$ and apply the following transformation to various parameters in the axial direction (the radial parameters remaining unaffected):

$$\begin{array}{ll} \bar{r} = \bar{R}, & \bar{u}\left(\bar{r}, \bar{z}\right) = \bar{U}\left(\bar{R}, \bar{Z} - c\bar{t}\right), \\ \bar{z} = \bar{Z} - c\bar{t}, & \bar{w}\left(\bar{r}, \bar{z}\right) = \bar{W}\left(\bar{R}, \bar{Z} - c\bar{t}\right) - c, \end{array} \tag{5}$$

where $\bar{u}$ and $\bar{w}$ are the velocity components in the wave frame.

Employing the transformations (5) in (3), using the following nondimensional quantities

$$\begin{array}{llll} r = \dfrac{\bar{r}}{h_0}, & z = \dfrac{2\pi\bar{z}}{\lambda}, & u = \dfrac{\bar{u}}{c}, & w = \dfrac{\bar{w}}{c}, \\ h = \dfrac{\bar{h}}{h_0}, & p = \dfrac{2\pi h_0^2 \bar{p}}{\lambda\mu c}, & t = \dfrac{2\pi c}{\lambda}\bar{t}, & \mathbf{S} = \dfrac{h_0}{\mu c}\bar{\mathbf{S}}, \end{array} \tag{6}$$

and introducing the stream function ψ and wavenumber δ by

$$u(r, z) = -\frac{\delta}{r}\frac{\partial\psi}{\partial z}, \quad w(r, z) = \frac{1}{r}\frac{\partial\psi}{\partial r}, \quad \delta = \frac{2\pi h_0}{\lambda}, \tag{7}$$

we find that $(3)_1$ is identically satisfied and $(3)_2$ for large wavelengths gives

$$-\frac{\partial p}{\partial r} = 0, \quad -\frac{\partial p}{\partial z} + \frac{1}{r}\frac{\partial}{\partial r}(r\tau_{rz}) = 0. \tag{8}$$

By employing (5)–(7), the constitutive equation (1) yields

$$\tau_{rz} = \frac{\alpha\dot{\gamma} + \beta\dot{\gamma}^3}{1 + \beta\dot{\gamma}^2}, \tag{9}$$

where the parameters α, β and the Weissenberg number $\mathcal{W}e$ are defined by

$$\alpha = \frac{\eta}{\mu} + 1, \quad \beta = \mathcal{W}e^2\left(1 - a^2\right), \quad \mathcal{W}e = \frac{mc}{h_0} \tag{10}$$

and the local shear rate $\dot{\gamma}$ is given by

$$\dot{\gamma} = \frac{\partial w}{\partial r} = \frac{\partial}{\partial r}\left(\frac{1}{r}\frac{\partial\psi}{\partial r}\right). \tag{11}$$

Equation $(8)_1$ shows that p is not a function of r. Hence, substituting (9) into $(8)_2$, we obtain

$$\frac{\mathrm{d}p}{\mathrm{d}z} = \frac{1}{r}\frac{\partial}{\partial r}\left(r\frac{\alpha\dot{\gamma} + \beta\dot{\gamma}^3}{1 + \beta\dot{\gamma}^2}\right). \tag{12}$$

Furthermore, eliminating the pressure between $(8)_1$ and $(8)_2$, we arrive at a differential equation for the stream function ψ

$$\frac{\partial}{\partial r}\left[\frac{1}{r}\frac{\partial}{\partial r}\left(\frac{\alpha r\dot{\gamma}+\beta r\dot{\gamma}^3}{1+\beta\dot{\gamma}^2}\right)\right]=0. \tag{13}$$

The nondimensional boundary conditions are [17]

$$\begin{aligned}&\psi=0, \quad \dot{\gamma}=0 \quad \text{at } r=0,\\ &\psi=F, \quad w=-1 \quad \text{at } r=h,\end{aligned} \tag{14}$$

where the nondimensional radius of the tube h is

$$h=1+\phi\sin z \tag{15}$$

with $\phi=b/h_0$ $(0<\phi<1)$ being the amplitude ratio or occlusion and $2\pi F$ indicated the nondimensional volume flux.

4 Perturbation solution

For small values of $\mathcal{W}e^2$ (12) and (13) application of the binomial theorem yields

$$\frac{\partial}{\partial r}\left\{\frac{1}{r}\frac{\partial}{\partial r}\left[r\left(\dot{\gamma}+\mathcal{W}e^2\alpha_1\dot{\gamma}^3+\mathcal{W}e^4\alpha_2\dot{\gamma}^5\right)\right]\right\}=0, \tag{16}$$

$$\frac{\mathrm{d}p}{\mathrm{d}z}=\alpha\frac{1}{r}\frac{\partial}{\partial r}\left[r\left(\dot{\gamma}+\mathcal{W}e^2\alpha_1\dot{\gamma}^3+\mathcal{W}e^4\alpha_2\dot{\gamma}^5\right)\right], \tag{17}$$

where

$$\alpha_1=\frac{\left(a^2-1\right)\eta}{(\eta+\mu)}, \quad \alpha_2=-\frac{\left(a^2-1\right)^2\mu}{(\eta+\mu)}. \tag{18}$$

In order to seek the solution of (16) and (17) with the boundary conditions (14) for small Weissenberg number, we expand ψ, F and p in the following form

$$\begin{aligned}&\psi=\psi_0+\mathcal{W}e^2\psi_1+\cdots, \quad (\dot{\gamma}=\dot{\gamma}_0+\mathcal{W}e^2\dot{\gamma}_1+\cdots,\ w=w_0+\mathcal{W}e^2w_1+\cdots),\\ &F=F_0+\mathcal{W}e^2F_1+\cdots, \quad p=p_0+\mathcal{W}e^2p_1+\cdots.\end{aligned} \tag{19}$$

Substituting (19) in (14), (16) and (17) and collecting terms with coefficients of like powers of $\mathcal{W}e^2$, we get the following set of equations:

Zeroth-order problem

$$\frac{\partial}{\partial r}\left[\frac{1}{r}\frac{\partial}{\partial r}(r\dot{\gamma}_0)\right]=0, \quad \frac{\mathrm{d}p_0}{\mathrm{d}z}=\alpha\frac{1}{r}\frac{\partial}{\partial r}(r\dot{\gamma}_0), \tag{20}$$

$$\begin{aligned}&\psi_0=0, \quad \dot{\gamma}_0=0 \quad &&\text{at } r=0,\\ &\psi_0=F_0, \quad w_0=-1 \quad &&\text{at } r=h.\end{aligned} \tag{21}$$

First-order problem

$$\frac{\partial}{\partial r}\left[\frac{1}{r}\frac{\partial}{\partial r}\left\{r(\dot{\gamma}_1+\alpha_1\dot{\gamma}_0^3)\right\}\right]=0, \quad \frac{\mathrm{d}p_1}{\mathrm{d}z}=\alpha\frac{1}{r}\frac{\partial}{\partial r}\left\{r(\dot{\gamma}_1+\alpha_1\dot{\gamma}_0^3)\right\}, \tag{22}$$

$$\begin{aligned}&\psi_1=0, \quad \dot{\gamma}_1=0 \quad &&\text{at } r=0,\\ &\psi_1=F_1, \quad w_1=0 \quad &&\text{at } r=h.\end{aligned} \tag{23}$$

Solving (20) subject to the boundary conditions (21), the zeroth-order expressions for the stream function, the axial velocity, the pressure gradient, and the pressure rise per wavelength $\left(\Delta P_{\lambda_0}\right)$ are, respectively, given by

$$\Psi_0 = \left(2F_0 + h^2\right)\left(L^2 - \frac{L^4}{2}\right) - \frac{r^2}{2}, \tag{24}$$

$$w_0 = \frac{2\left(2F_0 + h^2\right)}{h^2}\left(1 - L^2\right) - 1, \tag{25}$$

$$\frac{\mathrm{d}p_0}{\mathrm{d}z} = \frac{-8\alpha\left(2F_0 + h^2\right)}{h^4}, \tag{26}$$

$$\Delta P_{\lambda_0} = \int_0^{2\pi} \frac{\mathrm{d}p_0}{\mathrm{d}z}\mathrm{d}z = -8\alpha\left(I_2 + 2I_4F_0\right), \tag{27}$$

where $L = r/h$ and

$$I_2 = \frac{2\pi}{\left(1-\phi^2\right)^{3/2}}, \quad I_4 = \frac{\pi\left(3\phi^2+2\right)}{\left(1-\phi^2\right)^{7/2}}. \tag{28}$$

Solving (22) subject to the boundary conditions (23) and using the zeroth-order solution (24) for $\dot{\gamma}_0$, we get

$$\psi_1 = \frac{\alpha_1}{192}\left(\frac{\mathrm{d}p_0}{\mathrm{d}z}\right)^3\left[r^2h^4\left(2L^2 - L^4 - 1\right)\right] + F_1L^2\left(2 - L^2\right), \tag{29}$$

$$w_1 = \frac{\alpha_1}{192}\left(\frac{\mathrm{d}p_0}{\mathrm{d}z}\right)^3\left[h^4\left(8L^2 - 6L^4 - 2\right)\right] + \frac{4F_1}{h^2}\left(1 - L^2\right), \tag{30}$$

$$\frac{\mathrm{d}p_1}{\mathrm{d}z} = \frac{\alpha\alpha_1}{6}\left(\frac{\mathrm{d}p_0}{\mathrm{d}z}\right)^3 h^2 - \frac{16\alpha F_1}{h^4}, \tag{31}$$

$$\Delta P_{\lambda 1} = \frac{-256}{3}\alpha\alpha_1\left[8F_0^3I_{10} + 12F_0^3I_8 + 6F_0I_6 + I_4\right] - 16\alpha F_1I_4, \tag{32}$$

where

$$I_3 = \frac{\pi\left(2+\phi^2\right)}{\left(1-\phi^2\right)^{5/2}}, \quad I_k = \frac{1}{\left(1-\phi^2\right)}\left[\left(\frac{2k-3}{k-1}\right)I_{k-1} - \left(\frac{k-2}{k-1}\right)I_{k-2}\right], \qquad k > 4. \tag{33}$$

The expressions for ψ, w, $\mathrm{d}p/\mathrm{d}z$ and Δp_λ up to $\mathcal{W}e^2$ can now be written as

$$\begin{aligned}\psi = {} & \left(2F_0 + h^2\right)\left(L^2 - \frac{L^4}{2}\right) - \frac{r^2}{2} \\ & + \mathcal{W}e^2\left\{\frac{\alpha_1}{192}\left(\frac{\mathrm{d}p_0}{\mathrm{d}z}\right)^3\left[r^2h^4\left(2L^2 - L^4 - 1\right)\right] + F_1L^2\left(2 - L^2\right)\right\},\end{aligned} \tag{34}$$

$$\begin{aligned}w = {} & \frac{2\left(2F_0 + h^2\right)}{h^2}\left(1 - L^2\right) - 1 \\ & + \mathcal{W}e^2\left\{\frac{\alpha_1}{192}\left(\frac{\mathrm{d}p_0}{\mathrm{d}z}\right)^3\left[h^4\left(8L^2 - 6L^4 - 2\right)\right] + \frac{4F_1}{h^2}\left(1 - L^2\right)\right\},\end{aligned} \tag{35}$$

$$\frac{\mathrm{d}p}{\mathrm{d}z} = \frac{\mathrm{d}p_0}{\mathrm{d}z} + \mathcal{W}e^2\left\{\frac{\alpha\alpha_1}{6}\left(\frac{\mathrm{d}p_0}{\mathrm{d}z}\right)^3 h^2 - \frac{16\alpha F_1}{h^4}\right\}, \tag{36}$$

$$\begin{aligned}\Delta P_\lambda = {} & -8\alpha\left(I_2 + 2I_4F_0\right) \\ & + \mathcal{W}e^2\left\{\frac{-256}{3}\alpha\alpha_1\left[8F_0^3I_{10} + 12F_0^3I_8 + 6F_0I_6 + I_4\right] - 16\alpha F_1I_4\right\}.\end{aligned} \tag{37}$$

5 General solution

Integrating (13), we have

$$\frac{\alpha\dot{\gamma}+\beta\dot{\gamma}^3}{1+\beta\dot{\gamma}^2}=\frac{A(z)}{2}r+\frac{B(z)}{r}, \tag{38}$$

where $A(z)$ and $B(z)$ are functions of integration. In fact, by means of the expression (12) and the symmetric condition $(14)_2$, $\dot{\gamma}=0$ at $r=0$, we can immediately obtain $A(z)=\mathrm{d}p/\mathrm{d}z$ and $B(z)=0$. However, we abstain from specifying these functions of integration and prefer to work with the general form (38).

We utilize the transformation

$$\overline{\dot{\gamma}}=\beta\dot{\gamma}-\frac{\beta}{3}\left(\frac{A}{2}r+\frac{B}{r}\right). \tag{39}$$

This reduces (38) to

$$\overline{\dot{\gamma}}^3-3\widetilde{F}(r,z)\overline{\dot{\gamma}}-\widetilde{G}(r,z)=0, \tag{40}$$

where the functions $\widetilde{F}(r,z)$ and $\widetilde{G}(r,z)$ are given by the expressions

$$\begin{aligned}\widetilde{F}(r,z)&=\frac{\beta^2}{9}\left(\frac{A}{2}r+\frac{B}{r}\right)^2-\frac{\alpha\beta}{3},\\ \widetilde{G}(r,z)&=\beta^2\left(\frac{A}{2}r+\frac{B}{r}\right)\left(1-\frac{\alpha}{3}\right)+\frac{2}{27}\beta^3\left(\frac{A}{2}r+\frac{B}{r}\right)^3.\end{aligned} \tag{41}$$

The further substitution

$$\overline{\dot{\gamma}}=\widetilde{\delta}+\widetilde{\tau} \tag{42}$$

provides the solution of (40) in terms of $\widetilde{F}$ and $\widetilde{G}$ as

$$\begin{aligned}\widetilde{\delta}(r,z)&=\sqrt[3]{\frac{\widetilde{G}(r,z)}{2}+\frac{\sqrt{\widetilde{G}^2(r,z)-4\widetilde{F}^3(r,z)}}{2}},\\ \widetilde{\tau}(r,z)&=\sqrt[3]{\frac{\widetilde{G}(r,z)}{2}-\frac{\sqrt{\widetilde{G}^2(r,z)-4\widetilde{F}^3(r,z)}}{2}}.\end{aligned} \tag{43}$$

Note that since (40) is cubic in $\overline{\dot{\gamma}}$, one can have other solutions in addition to (42), viz.

$$\overline{\dot{\gamma}}=\widetilde{\omega}\widetilde{\delta}(r,z)+\widetilde{\omega}^2\widetilde{\tau}(r,z),\qquad \overline{\dot{\gamma}}=\widetilde{\omega}^2\widetilde{\delta}(r,z)+\widetilde{\omega}\widetilde{\tau}(r,z), \tag{44}$$

where $\widetilde{\omega}^3=1$.

We now invoke (39) on (42) to obtain

$$\dot{\gamma}=\frac{\widetilde{\delta}}{\beta}+\frac{\widetilde{\tau}}{\beta}+\frac{1}{3}\left(\frac{A}{2}r+\frac{B}{r}\right). \tag{45}$$

The integration of (45) yields the general solution for the stream function ψ

$$\psi(r,z)=\frac{1}{\beta}\int r\int\left[\widetilde{\delta}+\widetilde{\tau}\right]\mathrm{d}r\mathrm{d}r+\frac{1}{48}A(z)r^4+\frac{1}{3}B(z)\left[\frac{r^2}{2}\ln r-\frac{1}{4}r^2\right]+\frac{r^2}{2}C(z)+D(z), \tag{46}$$

where $A(z)$, $B(z)$, $C(z)$, and $D(z)$ are functions of integration that should be determined by the boundary conditions (14) and for which analytical expressions are impossible. Therefore, the analytical solution (46) can be obtained only by numerical methods. In the next section, we directly numerically solve the nonlinear boundary-value problem (13) and (14) instead of using the solution expression (46).

6 Numerical method

Here, instead of the approximate perturbation method described in Sect. 4 and the expression of the general analytical solution given in Sect. 5, we intend to find direct numerical solutions of the nonlinear differential equation (13) together with the boundary conditions (14) by means of a suitable numerical technique. For this purpose, we rewrite the differential equation (13) in the form

$$\frac{\partial}{\partial r}\left[\frac{1}{r}\frac{\partial}{\partial r}\left(\frac{(\alpha-1)r\dot{\gamma}}{1+\beta\dot{\gamma}^2}\right)\right]+\frac{\partial}{\partial r}\left[\frac{1}{r}\frac{\partial}{\partial r}\left(r\dot{\gamma}\right)\right]=0. \tag{47}$$

Because the differential equation (47) is nonlinear in $\dot{\gamma}$ (or ψ), we cannot solve this boundary-value problem by the direct finite-difference method. In solving such nonlinear equations, iterative methods are usually used.

We can now construct an iterative procedure for the local shear rate $\dot{\gamma}$ in the form

$$\frac{\partial}{\partial r}\left[\frac{1}{r}\frac{\partial}{\partial r}\left(\frac{(\alpha-1)r\dot{\gamma}^{(n+1)}}{1+\beta\left(\dot{\gamma}^{(n)}\right)^2}\right)\right]+\frac{\partial}{\partial r}\left[\frac{1}{r}\frac{\partial}{\partial r}\left(r\dot{\gamma}^{(n+1)}\right)\right]=0. \tag{48}$$

where the index n indicates the iterative step. If the indices n and $n+1$ are removed, (48) is consistent with (47). Substituting (10) and (11) into (48) yields an iterative procedure for the unknown ψ

$$\frac{\partial}{\partial r}\left[\frac{1}{r}\frac{\partial}{\partial r}\left(\frac{\left(\frac{\eta}{\mu}\right)r\frac{\partial}{\partial r}\left(\frac{1}{r}\frac{\partial\psi^{(n+1)}}{\partial r}\right)}{1+\mathcal{W}e^2\left(1-a^2\right)\left(\frac{\partial}{\partial r}\left(\frac{1}{r}\frac{\partial\psi^{(n)}}{\partial r}\right)\right)^2}\right)\right]+\frac{\partial}{\partial r}\left[\frac{1}{r}\frac{\partial}{\partial r}\left(r\frac{\partial}{\partial r}\left(\frac{1}{r}\frac{\partial\psi^{(n+1)}}{\partial r}\right)\right)\right]=0. \tag{49}$$

The Eq. (49) and the boundary conditions

$$\begin{aligned}&\psi^{(n+1)}=0,\quad \frac{\partial}{\partial r}\left(\frac{1}{r}\frac{\partial\psi^{(n+1)}}{\partial r}\right)=0 \ \text{ at } r=0,\\ &\psi^{(n+1)}=F,\quad \frac{1}{r}\frac{\partial\psi^{(n+1)}}{\partial r}=-1 \qquad \text{at } r=h\end{aligned} \tag{50}$$

define a linear differential boundary-value problem for $\psi^{(n+1)}$. By means of the finite-difference method a linear algebraic equation system can be deduced and solved for each iterative step. Therefore, a sequence of functions $\psi^{(0)}(r)$, $\psi^{(1)}(r)$, $\psi^{(2)}(r)$, ... is determined in the following manner: if $\psi^{(0)}(r)$ is given, then $\psi^{(1)}(r)$, $\psi^{(2)}(r)$, ... are calculated successively as the solutions of the boundary-value problem (49) and (50).

It should be pointed out that the choice of the iterative procedure (49) is not the only one possible. With this choice nothing can be asserted about the convergence of the sequence $\psi^{(n)}(r)$ to the solution $\psi(r)$ of the boundary-value problem; it can happen that the sequence does not converge. The effectiveness of the method is often influenced by the form of the arrangement (49) of the given differential equation. Convergence is also considerably influenced by the choice of the starting function $\psi^{(0)}(r)$; the method is generally more effective the closer $\psi^{(0)}(r)$ is to $\psi(r)$.

Usually, in order to achieve better convergence, the so-called method of successive under-relaxation is used. We solve the boundary-value problems (49) and (50) for the iterative step $n+1$ to obtain an estimated value of $\psi^{(n+1)}$: $\tilde{\psi}^{(n+1)}$, then $\psi^{(n+1)}$ is defined by the formula

$$\psi^{(n+1)}=\psi^{(n)}+\tau(\tilde{\psi}^{(n+1)}-\psi^{(n)}),\quad \tau\in(0,1], \tag{51}$$

where $\tau\in(0,1]$ is an under-relaxation parameter. We should choose τ so small that convergent iteration is reached. The iteration should be carried out until the relative differences of the computed $\psi^{(n+1)}$ and $\psi^{(n)}$ between two iterative steps are smaller than a given error, chosen to be 10^{-16}.

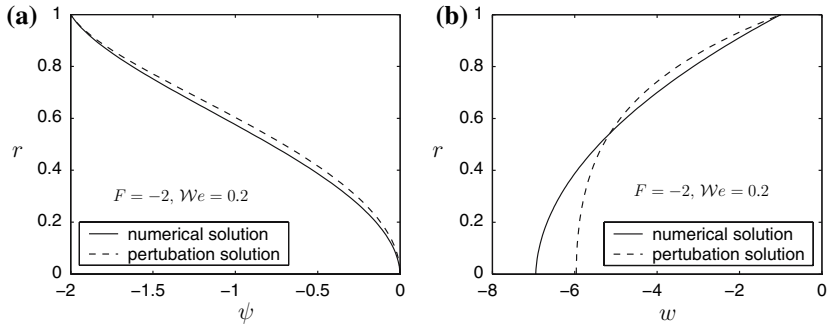

Fig. 2 Profiles of the dimensionless stream function $\psi(r)$ (**a**) and the velocity $w(r)$ (**b**). *Solid lines* indicate the numerical solutions of the boundary-value problem (13) and (14), while *broken lines* denote their approximate perturbation solutions. The other parameters are chosen as $F = -2$, $We = 0.2$, $h = 1$, $\mu/\eta = 1$, and $a = 0.8$

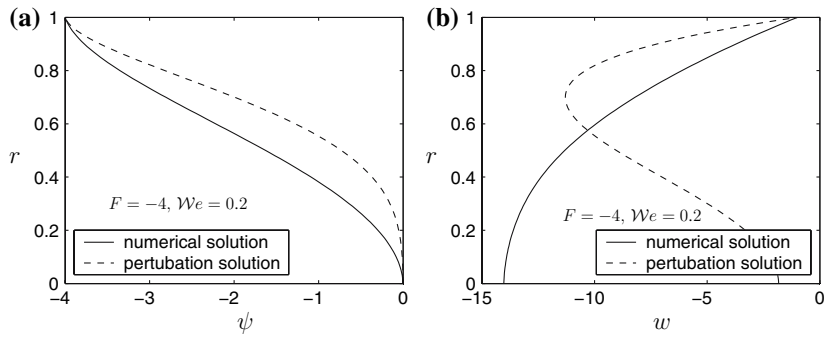

Fig. 3 As Fig. 2, but for a total flux of $F = -4$

7 Numerical results and discussions

A comparison of the direct numerical results as obtained for the boundary-value problem (13) and (14) and its approximate perturbation solutions to order We^2, (34) and (35), is shown in Figs. 2 and 3. We display the dimensionless stream function ψ (left panels) and the dimensionless axial velocity w obtained with two different values of the total flux, $F = -2$ in Fig. 2 and $F = -4$ in Fig. 3, respectively. For a Weissenberg number of $We = 0.2$ the difference between the approximate solutions and the direct numerical solutions is obvious. If the total flux increases from $F = -2$ in Fig. 2 to $F = -4$ in Fig. 3 their difference become more obvious. The reason is that the velocity profile deviates from a uniform distribution for $F = -4$ more than that for $F = -2$ and the term including We in (13) becomes more important. We will see later that for the boundary conditions (14) a total flux $F = 0.5$ yields a uniform velocity distribution, in which case the term containing the Weissenberg number in (13) vanishes and the magnitude of the Weissenberg number plays no role. Therefore, in this case the results of the approximate perturbation solutions will be in accordance with those of the direct numerical solutions, which hold for any value of We.

To quantitatively discriminate to what extent the perturbation solutions (34) and (35) can describe the boundary-value problem (13) and (14), an error measure for a physical variable φ, e.g., the stream function ψ or the velocity w, is introduced,

$$\mathcal{E}_\varphi = \sqrt{\frac{\sum_j \left(\varphi_j^{\text{app}} - \varphi_j^{\text{num}}\right)^2}{\sum_j \left(\varphi_j^{\text{num}}\right)^2}}, \tag{52}$$

where φ_j^{num} denotes the direct numerical solution at the space position y_j, whilst φ_j^{app} is the corresponding approximate value obtained by the perturbation solutions (34) and (35).

For various values of the Weissenberg number We the errors of the two solutions are listed in Table 1 for three different values of the total flux F. It is obvious that the errors increase with increasing Weissenberg

Table 1 Errors for the stream function ψ and the axial velocity w between the numerical solutions and the approximate perturbation solutions of the boundary-value problem (13) and (14) for different Weissenberg numbers $\mathcal{W}e$ and fluxes F

$\mathcal{W}e$		0.0	0.02	0.04	0.06	0.08	0.10	0.15	0.20
$F=-1$									
$\mathcal{E}_\psi$	[%]	0.37	0.48	0.46	0.79	1.14	1.27	1.41	1.65
$\mathcal{E}_u$	[%]	0.58	0.81	0.77	1.07	1.34	1.66	2.01	2.34
$F=-2$									
$\mathcal{E}_\psi$	[%]	0.35	0.51	0.76	1.02	1.27	1.63	1.90	2.63
$\mathcal{E}_u$	[%]	0.61	0.98	1.21	1.62	2.04	2.73	3.67	7.05
$F=-4$									
$\mathcal{E}_\psi$	[%]	0.51	1.03	1.83	2.17	2.42	3.76	12.18	23.19
$\mathcal{E}_u$	[%]	1.14	1.66	2.90	3.73	6.61	11.78	32.17	60.38

number $\mathcal{W}e$. For $F=-1$, up to $\mathcal{W}e=0.2$ or even larger, the perturbation solution is a good approximation, whilst for $F=-2$, if $\mathcal{W}e>0.2$, the approximate solutions can no longer be used. For a larger total flux value $F=-4$, the approximate perturbation solutions have to be abandoned even for very small values such as $\mathcal{W}e=0.1$. In these cases, in which the perturbation solution is no longer valid, this boundary-value problem must be solved by direct numerical methods.

Figure 4 shows the dependence of the flow on the Weissenberg number for two values of the total flux F. It can be seen that, for small values of the Weissenberg number, with an increase of $\mathcal{W}e$ the velocity profile along the transverse section becomes blunt, i.e., boundary thinning occurs. However, test computations show that the dependence of the velocity profile on the Weissenberg number is not monotonic. For $F=-2$ the largest deviation of the velocity profile from its distribution of a Newtonian fluid ($\mathcal{W}e=0$) occurs with $\mathcal{W}e=0.3$, whilst for $F=-4$ the largest deviation is achieved with $\mathcal{W}e=0.2$. A further increase of the Weissenberg number will make the corresponding deviation smaller, and hence for very large values of $\mathcal{W}e$ the behavior of a Johnson–Segalman fluid with reference to this considered flow case tends again to that of a Newtonian fluid. The reason for this is that, with increasing $\mathcal{W}e$, the denominator of the first term on the left-hand side of (13) becomes larger, and hence the second term becomes more dominant. In such cases the solution of (13) at large $\mathcal{W}e$ tends to the solution of a Newtonian fluid ($\mathcal{W}e=0$) again.

In Fig. 5 the distributions of the stream function $\psi(r)$ and the velocity $w(r)$ are illustrated for various values of the total flux F. Results are obtained by the direct numerical method, because here we choose a value of $\mathcal{W}e=0.1$ and hence the perturbation solutions may bring large errors for large values of F. Obviously, the flow is dominantly influenced by the value of F. For a tube radius of $h=1$, if $F=-0.5$, a constant velocity distribution across the cross-section is formed; in this case, no pressure gradient exists near the cross-section of $h=1$. If $F>-0.5$, the flow velocity profile is curved toward the positive z-direction (not shown in Fig. 5) due to an exerted pressure gradient in the negative z-direction, whilst for $F<-0.5$ a pressure gradient in the positive z-direction is required to maintain such a flux value, hence the flow velocity is curved toward the negative z-direction.

The distributions of the pressure gradient $\mathrm{d}p/\mathrm{d}z$ within a wavelength $z\in[0,2\pi]$ are shown in Fig. 6 for various values of the dimensionless wave amplitude ϕ, in Fig. 7 for various values of the total flux F, and in

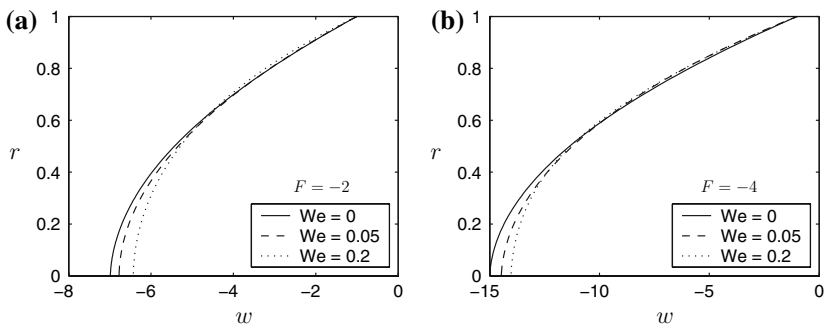

Fig. 4 Profiles of the dimensionless axial velocity $w(r)$ for two different values of the total flux $F=-2$ (*left panel*) and $F=-4$ (*right panel*) simulated for various values of the Weissenberg number, respectively. The other parameters are: $h=1$, $\mu/\eta=1$, and $a=0.8$

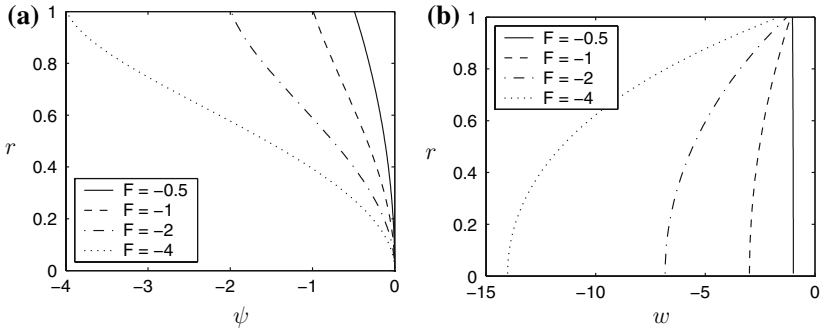

Fig. 5 Profiles of the dimensionless stream function $\psi(r)$ (**a**) and velocity $w(r)$ (**b**) simulated for various values of the total flux $F = -0.5, -1.0, -2.0$, and -4.0. The other parameters are $h = 1$, $\mu/\eta = 1$, $a = 0.8$, and $\mathcal{W}e = 0.1$

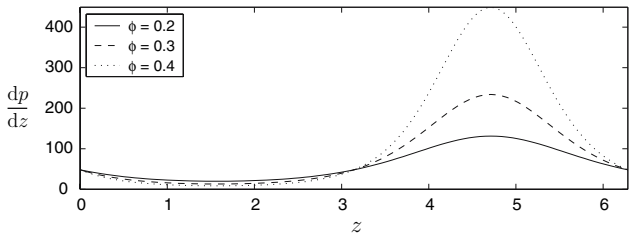

Fig. 6 Distributions of the pressure gradient $\mathrm{d}p/\mathrm{d}z$ within a wavelength $z \in [0, 2\pi]$ for different values of the amplitude ratio ϕ. The other parameters are $F = -2$, $\mu/\eta = 1$, $a = 0.8$, and $\mathcal{W}e = 0.1$

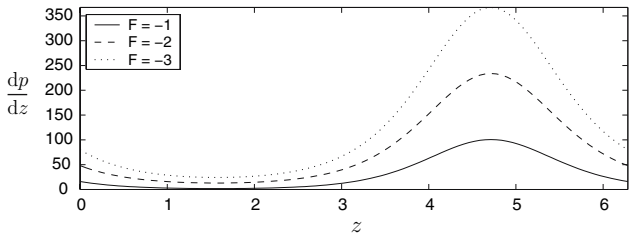

Fig. 7 Distributions of the pressure gradient $\mathrm{d}p/\mathrm{d}z$ within a wavelength $z \in [0, 2\pi]$ for different values of the total flux F. The other parameters are $\phi = 0.3$, $\mu/\eta = 1$, $a = 0.8$, and $\mathcal{W}e = 0.1$

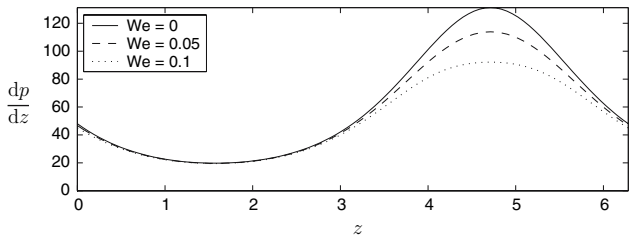

Fig. 8 Distributions of the pressure gradient $\mathrm{d}p/\mathrm{d}z$ within a wavelength $z \in [0, 2\pi]$ for different values of the Weissenberg number $\mathcal{W}e$. The other parameters are $F = -2$, $\phi = 0.2$, $\mu/\eta = 1$, and $a = 0.8$

Fig. 8 for various values of the Weissenberg number $\mathcal{W}e$. The dimensionless tube radius is defined by (15), i.e., $h(z) = 1 + \phi \sin z$. The results are obtained by directly solving the boundary-value problem (13) and (14) for various values of the tube radius h within a wavelength and then substituting the results into (12) to obtain the pressure gradient at various points along the tube.

It can be clearly seen from Figs. 6, 7 and 8 that, on the one hand, in most of the channel, $z \in [0, \pi]$, the pressure gradient is relatively small, i.e., the flow can easily pass without the imposition of a large pressure gradient. On the other hand, in a narrow part of the channel, $z \in [\pi, 2\pi]$, a much larger pressure gradient is required to maintain the same flux to pass it, especially for the narrowest position near $z = 3\pi/2$ and when

Table 2 Pressure drop per wavelength in the longitudinal direction for various values of the total flux F and wave amplitude ϕ

F		1.0			−0.5			−2.0			−4.0	
ϕ	0.2	0.3	0.4	0.2	0.3	0.4	0.2	0.3	0.4	0.2	0.3	0.4
$\triangle P_\lambda$	−353	−432	−587	16	41	98	383	518	787	877	1153	1704

The other parameters are: $\mu/\eta = 1$, $a = 0.8$, and $\mathcal{W}e = 0.02$

the wave amplitude ϕ (Fig. 6) or the absolute value of the flux F (Fig. 7) is larger. When the effect of the Weissenberg number becomes more important (with its increase for small $\mathcal{W}e$ values or with its decrease for large $\mathcal{W}e$ values), a smaller pressure gradient is needed to maintain the flow through the narrow part of the tube due to the effect of boundary thinning and the consequent resistance reduction, as seen in Fig. 8.

The corresponding pressure drops in the flow direction over a wavelength are listed in Table 2 for some values of F and ϕ. These are still obtained by the perturbation method, i.e., (37), due to the small value of $\mathcal{W}e = 0.02$ used. For small values of F, a pressure rise occurs in the flow direction. With the increase of the flux F and the wave amplitude ϕ, the pressure drops increase over a wavelength.

8 Conclusions

Plane steady peristaltic motions of a Johnson–Segalman fluid were analyzed for the conditions that the tube is sinusoidally deformed. The tube deformation has a wavelength λ that is large in comparison to the undeformed tube radius and propagates at a prescribed constant speed c. A scale analysis and associated nondimensionalization of the equations paired with a Galilei transformation with speed c discloses a steady time-independent problem in which an aspect-ratio parameter δ and the Weissenberg number $\mathcal{W}e$ appear as the significant physical scales. The equations in the limit $\delta \to 0$ describe the large-wavelength approximation. These equations still contain the Weissenberg number $\mathcal{W}e$ as a parameter. Perturbation solutions up to $\mathcal{O}\left(\mathcal{W}e^2\right)$ for the investigated flow were constructed for a prescribed total flux F and were compared with numerical solutions valid for any value of the Weissenberg number. The findings are summarized as follows:

- Qualitatively, the axisymmetric flow case in a tube is similar to the two-dimensional channel-flow case investigated in [22], but quantitatively the two cases are different. The analysis of the cylindrical case requires extensive algebraic manipulation.
- A major object of the present analysis of peristaltic flows through a tube is to relate peristaltic flow and the spurt phenomenon, which has not been explained in the literature yet. Spurt is the term used to describe the large increase in the volume throughput for a small increase in the driving pressure gradient that is observed in the flow of a Johnson–Segalman fluid model. Experimentalists usually associate this phenomenon with slip at the wall. The Johnson–Segalman model offers a very interesting means for explaining spurt; it seems more likely that the phenomenon is due to the stick–slip phenomenon that takes place at the boundary. However, this model could very well describe the shear layers.
- The deviation of the flow from a constant velocity profile depends on both the flux F and the Weissenberg number $\mathcal{W}e$. For $F = -0.5$, the nonlinear viscous properties do not enter the flow at the position with a tube radius of $h = 1$ no matter how large $\mathcal{W}e$ is.
- With growing deviation of F from $F = -0.5$ for the position with a tube radius of $h = 1$ the influence of the nonlinear viscous properties of the fluid becomes increasingly significant.
- The profiles of the stream functions and the longitudinal velocities as computed using the perturbation expansion are only adequately predicted when the Weissenberg number $\mathcal{W}e$ is very small. The maximum values for which the perturbation solutions are valid approximations depend on the flux variable F, and become larger as F deviates from -0.5.
- For a given total flux a Weissenberg number $\mathcal{W}e$ exists for which the maximum deviation from the velocity distribution of the Newtonian fluid ($\mathcal{W}e = 0$) is reached, e.g., $\mathcal{W}e = 0.3$ for $F = -2$ and $\mathcal{W}e = 0.2$ for $F = -4$ at a position with tube radius $h = 1$, for which the effect of the boundary thinning is most obvious.
- The effect of boundary thinning causes the flow resistance to become smaller.

Acknowledgments Comments by two anonymous referees of this manuscript are greatly appreciated.

References

1. Latham, T.W.: Fluid motion in a peristaltic pump. MS Thesis, M III Cambridge, Mass (1966)
2. Jafrin, M.Y., Shapiro, A.H.: Peristaltic pumping. Ann. Rev. Fluid Mech. **3**, 13–35 (1971)
3. Burns, J.C., Parkes, J.: Peristaltic motion. J. Fluid Mech. **29**, 731–743 (1967)
4. Barton, C., Raymor, S.: Peristaltic flows in tubes. Bull. Math. Bio. Phy. **30**, 663–680 (1968)
5. Chow, T.S.: Peristaltic transport in a circular cylindrical pipe. J. Appl. Mech. **37**, 901–906 (1970)
6. Shapiro, A.H., Jaffrin, M.Y., Weinberg, S.L.: Peristaltic pumping with long wavelength at low Roynolds number. J. Fluid Mech. **37**, 799–825 (1969)
7. Jaffrin, M.Y.: Inertia and streamline curvature effects on peristaltic pumping. Int. J. Eng. Sci. **11**, 681–699 (1973)
8. Liron, N.: On peristaltic flow and its efficiency. Bull. Math. Biol. **38**, 573–596 (1976)
9. Takabatake, S., Ayukawa, K.: Numerical study of two-dimensional peristaltic flows. J. Fluid Mech. **122**, 439–465 (1982)
10. Radhakrishnamacharya, G.: Long wavelength approximation to peristaltic motion of power law fluid. Rheol. Acta **21**, 30–35 (1982)
11. Raju, K.K., Devanathan, R.: Peristaltic motion of a non-Newtonian fluid. Rheol. Acta **11**, 170–178 (1972)
12. Raju, K.K., Devanathan, R.: Peristaltic motion of a non-Newtonian fluid, Part II. Viscoelastic fluid. Rheol. Acta **13**, 944–948 (1974)
13. Srivastava, L.M.: Peristaltic transport of a couple stress fluid. Rheol. Acta **25**, 638–641 (1986)
14. Srivastava, L.M., Srivastava, V.P.: Peristaltic transport of a power law fluid: application to the ductus efferentes of the reproductive tracts. Rheol. Acta **27**, 428–433 (1988)
15. Siddiqui, A.M., Provost, A., Schwarz, W.H.: Peristaltic pumping of a second order fluid in a planar channel. Rheol. Acta **30**, 249–262 (1991)
16. Siddiqui, A.M., Schwarz, W.H.: Peristaltic pumping of a third order fluid in a planar channal. Rheol. Acta **32**, 47–56 (1993)
17. Siddiqui, A.M., Schwarz, W.H.: Peristaltic flow of a second order fluid in tubes. J. Non-Newton. Fluid Mech. **53**, 257–284 (1994)
18. Böhme, G., Friedrich, R.: Peristaltic flow of viscoelastic liquids. J. Fluid Mech. **128**, 109–122 (1983)
19. Misra, J.C., Pandey, S.K.: Peristaltic transport of a non-Newtonian fluid with a peripheral layer. Int. J. Eng. Sci. **37**, 1841–1858 (1999)
20. Misra, J.C., Pandey, S.K.: Peristaltic flow of a multilayered power-law fluid through a cylindrical tube. Int. J. Eng. Sci. **39**, 387–402 (2001)
21. Hayat, T., Wang, Y., Siddiqui, A.M., Hutter, K., Asghar, S.: Peristaltic transport of a third order fluid in a circular cylindrical tube. Math. Models Methods Appl. Sci. **12**(12), 1691–1706 (2002)
22. Hayat, T., Wang, Y., Siddiqui, A.M., Hutter, K.: Peristaltic motion of a Johnson–Segalman fluid in a planar channel. Math. Probl. Eng. **2003**(1), 1–23 (2003)
23. Kolkka, R.W., Malkus, D.S., Hansen, M.G., Ierly, G.R., Worthing, R.A.: Spurt phenomenon of the Johnson–Segalman fluid and related models. J. Non-Newton. Fluid Mech. **29**, 303–335 (1988)
24. McLeish, T.C.B., Ball, R.C.: A molecular approach to the spurt effect in polymer melt flow. J. Polym. Sci. (B) **24**, 1735–1745 (1986)
25. Malkus, D.S., Nohel, J.A., Plohr, B.J.: Dynamics of shear flow of a non-Newtonian fluid. J. Comput. Phys. **87**, 464–487 (1990)
26. Malkus, D.S., Nohel, J.A., Plohr, B.J.: Analysis of new phenomenon in shear flow of non-Newtonian fluids. SIAM J. Appl. Math. **51**, 899–929 (1991)
27. Migler, K.B., Hervert, H., Leger, L.: Slip transition of a polymer melt under shear stress. Phys. Rev. Lett. **70**, 287–290 (1990)
28. Migler, K.B., Massey, G., Hervert, H., Leger, L.: The slip transition at the polymer-solid interface. J. Phys. Condens. Matter A **6**, 301–304 (1994)
29. Ramamurthy, A.V.: Wall slip in viscous fluids and the influence of material of construction. J. Rheol. **30**, 337–357 (1986)
30. Kraynik, M., Schowalter, W.R.: Slip at the wall and extrudate roughness with aqueous solutions of polyvinyl alcohal and sodium borate. J. Rheol. **25**, 95–114 (1981)
31. Lim, F.J., Schowalter, W.R.: Wall slip of narrow molecular weight distribution polybutadienes. J. Rheol. A. **33**, 1359–1382 (1989)
32. Johnson, M.W. Jr., Segalman, D.: A model for viscoelastic fluid behaviour which allows non-affine deformation. J. Non-Newton. Fluid Mech. **2**, 255–270 (1977)